Technical Paper

ISSN 1997-1400 Int. J. Pavement Res. Technol. 4(3):168-175

Experimental Investigation of Aggregate-Mortar Interface Affecting the Early Fracture Toughness of Portland Cement Concrete

Tongyan Pan[1+], Linbing Wang[2], and Erol Tutumluer[3]

Abstract: The paper presents the research findings from a laboratory experimental study directed at investigating the size and morphological effects of aggregate materials on the response of young concrete under tensile stress. Six concrete specimens were fabricated using aggregate materials of different morphologies, sizes and gradations. Concrete fracture toughness in terms of the specific fracture energy (G_F) from a wedge split test configuration was determined to characterize the concrete cracking behavior at the age of twelve hours after specimen-casting. Using an image analysis approach, two important aggregate morphological indices, i.e., an angularity index (*AI*) and a surface texture index (*ST*) were defined to accurately quantify the angularity and surface texture properties of the aggregate particles that were used in the six concrete specimens. The total surface area of all the aggregate particles in each specimen was determined using the image analysis technology. Best-fit regression analyses were performed that linked the G_F to the *AI* and *ST* indices, the maximum aggregate size and surface area of aggregate materials. The observations from this study was finally explained in terms of the interfacial transition zone (ITZ) as the critical place where early age cracking of concrete tend to initiate and propagate under tensile stress.

Key words: *Aggregate; Concrete cracking; Fracture toughness; Image analysis; Interfacial transition zone.*

Introduction

Large-size concrete structural components experience thermal and drying deformations within twenty-four hours of casting when they are restrained by adjacent structures, gravity, or friction from the underlying soil. Thermal and moisture gradients generated during cement hydration can induce stresses high enough to cause cracking in the concrete due to the concrete's low tensile strength and fracture toughness. Deformations caused by various types of early age shrinkages, such as the plastic shrinkage and chemical shrinkage also impose additional stress in the structure and add to concrete cracking in early age [1]. Early-age deformations can lead to poor load transfer efficiency across joints or cracks. Tensile cracking in concrete slabs propagates under mode I fracture, which can be simulated in the laboratory using the three-point bend or wedge-split test configuration. An effective way to characterize the fracture behavior of concrete is to measure the amount of energy required to fully crack the specimen, i.e., the fracture toughness in terms of measured specific fracture energy - G_F [2].

Hydrated cement concrete is a three-phase composite material that includes the cement paste, aggregate and the interfacial transition zone (ITZ) between the paste and aggregate particles. The fracture toughness of a concrete structure mainly depends on the mechanical properties of these three components. Aggregate materials compose the bulk of concrete and aggregate shape, size and gradation affect the performance of concrete [3]. Mixes containing angular particles were reported to produce higher strength and modulus values compared to those including gravel only [4]. However the aggregate size and morphological properties do not often receive enough consideration in mixture design due to the comparatively strong and stable aggregate strength and toughness before and after the concrete casting. Moreover, use of rounded-shape particles in concrete mixes is preferred in practice to avoid crushing and increased paste expenses.

Although the aggregate materials per se possess stable mechanical properties throughout the life cycles of concrete structures, they have been found to affect the strength and toughness of the aggregate-paste bond. Extensive research studies have found that the early-age bond strength was much lower than the strengths of both aggregate and cement paste [5, 6]. The aggregate size and morphological properties such as surface texture and specific area were also reported as related to the early-age bond strength of concrete [6-8]. However, the relationship between the aggregate morphology and the aggregate-paste bond strength which in turn may determines the strength of concrete is not well understood due to the lack of quantitative measurements of coarse aggregate morphology [9].

Moreover, an effective study of the aggregate – paste bond strength in a concrete structure requires the accurate measure of the surface area of the individual aggregate particles [8, 9]. Previous studies on the aggregate-paste mechanical properties were mainly conducted by casting cement paste on the precut surface of rock blocks [6, 8, 10], which neglected the effects of aggregate particles on the paste by increasing the local rates of shearing and may allow the particles to acquire a coating of cement grains while moving through the paste during mixing. Using precut rock blocks in studying ITZ may also result in an extensive surface that facilitates

[1] Assistant Professor, Department of Civil Engineering, The Catholic University of America, Washington, DC 20064, USA.
[2] Associate Professor, Department of Civil and Environmental Engineering, Virginia Polytechnic Institute and State University, Blacksburg, Virginia 24060, USA.
[3] Professor, Department of Civil and Environmental Engineering, University of Illinois at Urbana-Champaign, Urbana, IL 60801, USA.
[+] Corresponding Author: E-mail tongyanpan@gmail.com
Note: Submitted June 10, 2010; Revised August 25, 2010; Accepted August 27, 2010.

the formation of a water film and bleeding [9]. Accordingly, the availability of an effective means to measure the coarse aggregate surface area will no doubt facilitate the study of aggregate – paste bond strength in concrete structures.

During the past couple of decades, owing to the objective measurements taken in an automated means using the advanced imaging technology, aggregate morphology studies based on image analysis have been successfully conducted and the various imaging based aggregate morphological indices have been linked to material strength and deformation properties as well as to results from manual testing methods in recent years [11]. Among the promising aggregate imaging systems, University of Illinois Aggregate Image Analyzer (UIAIA) is an integrated 3-D system developed recently to provide an automated means to determine coarse aggregate size and shape properties. Among the key particle morphological or shape indices developed in the UIAIA system, the angularity index (*AI*) and surface texture (*ST*) index are two indices that have been recently validated by successfully measuring aggregate properties and linking results to corresponding laboratory strength data and field performances [12-16]. Recent advances for quantifying three-dimensional shape of aggregate particles have also been completed in the framework of UIAIA. An algorithm is developed in the UIAIA system for measuring the surface area of individual aggregate particles.

With accurate measurement of the angularity and surface texture properties, as well as the surface area of irregular shaped aggregate particles using image analysis, the effects of aggregate shape or morphological properties on the early age cracking behavior can be more readily studied. This study presents the research findings recently made at the University of Illinois in quantifying the aggregate particle morphology, and linking them to the fracture energy to better understand the early age cracking behavior of Portland cement concrete.

Objectives and Scopes

The main objective of this study is to investigate the possible effects of aggregate size and shape properties on the early age cracking behavior of concrete structures such as pavement slabs using the results of concrete fracture energy tests. The imaging based *AI* and *ST* indices, maximum aggregate size and the surface area of aggregate particles are linked to the fracture energy of concrete specimens fabricated and tested in the laboratory. The following tasks were conducted to meet the above objective: (1) developing an algorithms in UIAIA system to determine *AI* and *ST* indices, as well as the total surface area of aggregate particles included in each specimen, (2) fabricating and testing the concrete specimens to collect the fracture energy data, and finally, (3) analyzing for possible morphological properties of aggregate that affect the early-age cracking behavior of concrete.

Imaging Based Aggregate Morphological Indices

Both the *AI* and *ST* indices as defined in the UIAIA system were developed based on three orthogonally acquired two-dimensional (2-D) images for each aggregate particle. The imaging based angularity index *AI* in UIAIA measures the angularity property of an aggregate particle by directly counting the relative differences of the adjacent vertex angles of the n-sided polygon that is determined to best approximate the profile of the particle as illustrated in Fig. 1(a). On the other aspect, the imaging based surface texture *ST* index was developed to quantify the average depth of surface irregularities of a particle, of which the scale is too small for the *AI* to measure. The algorithms involved in the *AI* and the *ST* indices are introduced next.

Angularity Index (*AI*)

To approximate the profile of each 2-D image of a particle, the coordinates of the profile are extracted first. Then, the outline is approximated by an n-sided polygon as shown in Fig. 1(a). An optimum n value of 24 has been determined to best separate the typical *AI* values of the crushed particles from those of the uncrushed gravel. The angle subtended at each vertex of the polygon is computed next. A relative change in slope of the n sides of the polygon is subsequently estimated by computing the change in angle (α) at each vertex with respect to the angle in the preceding vertex. The frequency distribution of the changes in the vertex angles is established in 10-degree class intervals. The number of occurrences in a certain interval and the magnitude are then related to the angularity of the particle.

Eq. (1) is used for calculating *Angularity* of each projected image. In this equation, e is the starting angle value for each 10-degree class interval and $P(e)$ is the probability that change in angle α_n has a value in the range e to $(e+10)$.

$$Angularity, \quad A = \sum_{e=0}^{170} e \times P(e) \tag{1}$$

The *Angularity Index, AI* of a particle is then determined by averaging the *Angularity* values as per Eq. (1) calculated from all three views when weighted by their areas as given in the following equation:

$$AI = \frac{\sum_{i=1}^{3} (Angularity_i \times Area_i)}{\sum_{i=1}^{3} Area_i} \tag{2}$$

where, i takes values from 1 to 3 for top, front, and side orthogonal views. The final *AI* value for the entire sample is simply an average of the *Angularity* values of all the particles weighted by the particle weight, which measures overall degree changes on the boundary of a particle. From its definition as given in Eq. (2), the *AI* has the same degree unit as an angle does.

Surface Texture (*ST*)

The UIAIA Surface Texture (*ST*) index was defined based on the image analysis technique “erosion and dilation.” One erosion cycle processes each 2-D image by removing boundary pixels off an object surface to leave the object less dense along its outer boundary. Dilation on the other hand is the reverse process of erosion and a

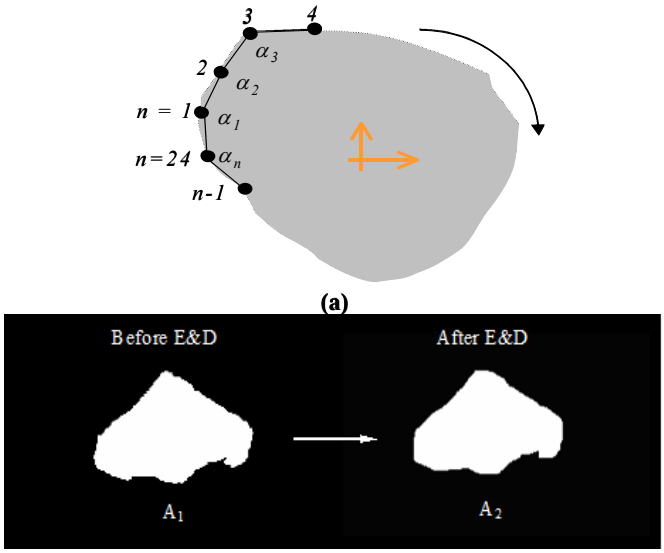

Fig. 1. (a) Illustration of An *n*-sided Polygon Approximating the Outline of an Aggregate Particle; (b) Change of the Particle Surface Texture before and after the Optimum Cycles of Erosion and Dilation.

single dilation cycle increases the particle shape or image dimension by the same pixels around its boundary. Erosion cycles followed by the same number of dilation cycles tend to smooth the surface of a particle by trimming the peaks and corners and patching the sharp dents on the boundary. In essence, the imaging pixel count based area difference of the 2-D image before and after the erosion and dilation cycles of the same number of cycles is directly related to the surface micro-irregularities, which defines the *st* for one of the three particle projection images per Eq. (3).

$$st = \frac{A_1 - A_2}{A_1} \times 100 \tag{3}$$

where

st = Surface texture parameter for each 2-D image;

A_1 = Area (in pixels) of the 2-D projection of the particle in the image;

A_2 = Area (in pixels) of the particle after performing a sequence of "*n*" cycles of erosion followed by "*n*" cycles of dilation.

Similar to the definition of the *AI*, the image analysis procedure first provides an *st* value for each of the three images obtained from three orthogonal views. Next, a particle index, denoted as *ST*, is established for the particle by taking a weighted average of each *st* determined from all three views.

To set up an *st* index independent of particle size, the optimum number of cycles of erosion and dilation, *n*, to be applied can be obtained as follows:

$$n = \frac{L}{\beta} \tag{4}$$

where

L = Longest or maximum intercept of a particle in image;

β = Scaling factor for erosion and dilation operations.

The optimal *n* value is determined as 20 at which *ST* of a set of smooth surface coarse aggregate is recognized as significantly separated from the *ST* of a set of rough surface coarse aggregate. The effect of optimum cycles of erosion and dilation on the surface irregularities can be illustrated in Fig. 1(b).

The final aggregate surface texture, *ST*, which measures the overall surface irregularities of a particle, is computed as the weighted average of each *st* determined from all three views as shown in Eq. (5). Unlike the *AI* that has a unit of an angle, the *ST* is a dimensionless quantity, as it measures the ratio of the areas before and after erosion and dilation cycles.

$$ST = \frac{\sum_{i=1}^{3}(st_i \times Area_i)}{\sum_{i=1}^{3} Area_i} \tag{5}$$

where *i* takes values from 1 to 3 for the top, front, and side orthogonal views.

The resolution of the 2-D images used in capturing aggregate particle images influences the *AI* and *ST* values. The sample size of the aggregate particles also has an important effect on the *AI* and *ST* values. In determining the *AI* and *ST* indices that can significantly separate coarse aggregates with smooth surfaces from those with rough surfaces, a statistically sufficient number of uncrushed gravel particles should be processed in an aggregate sample to represent coarse aggregates with smooth surfaces. Another set of statistically sufficient number of particles of crushed granite is also needed to form the sample of the rough surfaced coarse aggregates.

Surface Area Determination of Aggregate Particles

Surface area computation of an individual irregular-shaped particle is accomplished in the UIAIA image analysis system based on the three-dimensional (3-D) reconstruction of the particle as an assembly of cubic volume units (voxels) [17]. The surface area of the aggregate can be determined as a summation of the surface layer of the voxels. In UIAIA system, three orthogonal two-dimensional (2-D) projection views are captured for an individual particle as shown in Fig. 2(a) using three orthogonally positioned digital cameras. The 3-D reconstruction of the particle is then performed in a rectangular framework as shown in Fig. 2(b), which is extracted from the three views as the smallest one to contain the particle.

The reconstruction of a 3-D aggregate particle using three orthogonal projection images is performed in a reverse tracking mode as illustrated in Fig. 3. Any component voxel of the aggregate particle has three 2-D projections, each in one of the three coordinate planes, i.e. *XYO, OYZ* and *XOZ* planes. Each projection is a 2-D square shaped element commonly referred to as a pixel. The three projected pixels of a voxel have coordinates corresponding to those of the voxel in the 3-D space in the following way (Fig. 3): A voxel with coordinates of (a, b, c) has a projected pixel in the *XYO* coordinate plane with the coordinates of (a, b, 0), a projected pixel in the *OYZ* coordinate plane with the coordinates of (0, b, c) and a projected pixel in the *XOZ* coordinate plane with the coordinates of (a, 0, c). Therefore once the coordinates of a voxel are given, the coordinates of its three

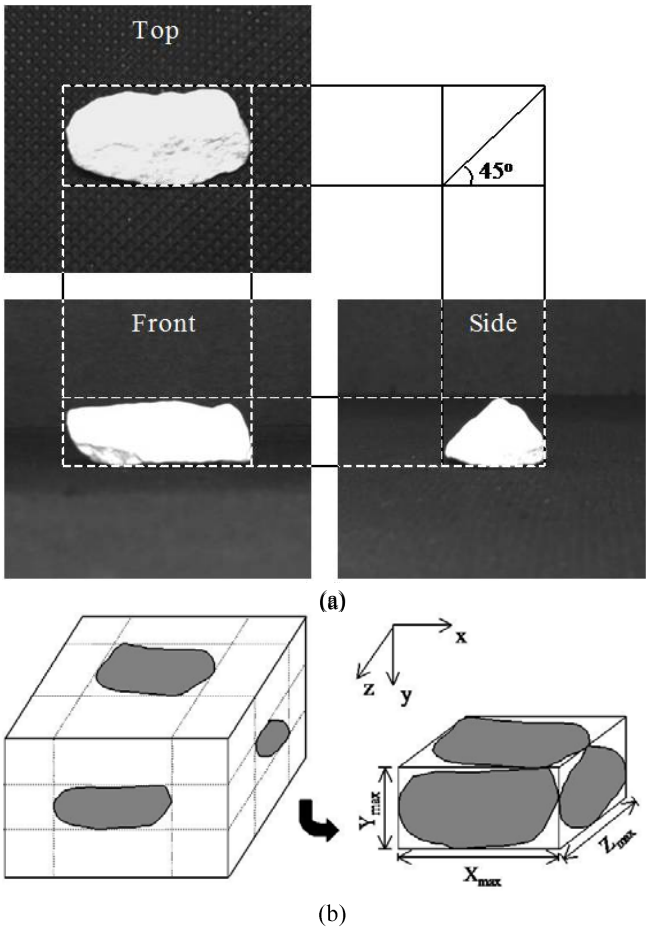

Fig. 2. (a) Three Orthogonal Views of a Particle Captured by the UIAIA; (b) Smallest Rectangular Framework Determined for Containing an Aggregate Particle.

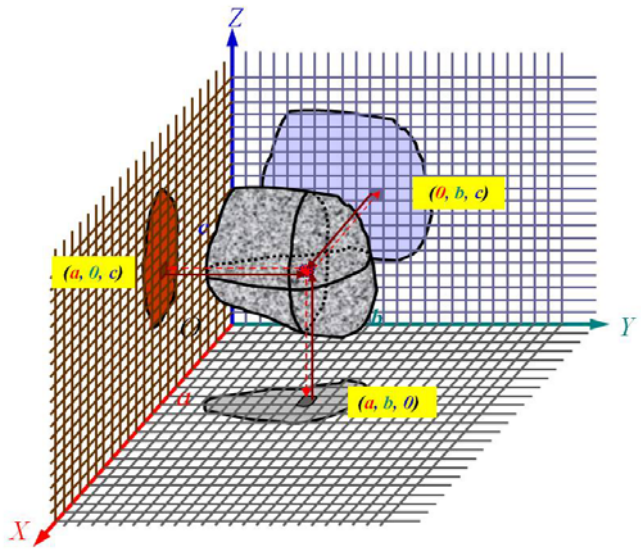

Fig. 3. Illustration of the Reverse Tracking Mode for Reconstructing an Aggregate Particle.

projection pixels can be determined accordingly, and vice versa. The one-to-one correspondence between any component voxel in the 3-D rectangular framework and its three projection pixels forms the basis of the reverse tracking mode used in reconstructing the 3-D aggregate particle from the orthogonal projection images.

Once the location of the individual component voxels of the rectangular framework is determined by the coordinates of their projection pixels, the component voxels belonging to the aggregate part in the rectangular framework can be recognized through checking the intensity values of each voxel of the rectangular framework. A voxel that belongs to the aggregate part in the 3-D rectangular framework has an intensity value of 255 as compared to the intensity value of 0 for those voxels in the 3-D rectangular framework but do not belong to aggregate part (Fig. 2(b)). The intensity value of a voxel is defined through the intensity values of its three projected pixels in the way that a combination of any three pixels that all have the intensity of 255, and satisfy the coordinate specification according to the principle detailed in last paragraph correspond to a voxel that belongs to the particle part in the 3-D framework. The surface area of an aggregate particle is calculated by summing up the surface layer of voxels of the particle in the 3-D rectangular framework according to Eq. (6) by a UIAIA Program. The surface area in terms of voxels is then converted to a value of commonly used units like squared meters, or squared inches etc., through calibration.

$$SA = \iint_{\Omega} ds = \lim_{n\to\infty} \sum_{i=1}^{n} \Delta S_i = \sum voxel_{surface} \tag{6}$$

where, SA is surface area of the aggregate particle; Ω is the particle surface; ds and ΔS_i is the surface area element; and $voxel_{surface}$ is the voxels in particle surface.

Resolution of the three cameras used in 2-D images acquisition significantly affects the surface area results. The higher the resolution level is used, the more accurate surface area result will be. In this study, a high resolution level 3,200×2,400 pixels per image is used, in which each square pixel has the side length of 32 μm. It should be noted that surface micro irregularities in the texture scale that have dimensions lower than 32 μm cannot be resolved using the 3,200×2,400 pixels resolution, which results in an underestimate of the surface area magnitude.

Laboratory Fracture Energy Determination

Fracture toughness of concrete was determined in terms of the specific fracture energy G_F that measures the work required to cause the initiation and propagation of a unit crack. The fracture energy is calculated for the wedge-split test (WST) specimen considering three force components acting on the WST specimen, i.e., the vertical force F_V, horizontal force F_H, and the sample weight (mg) as shown in Fig. 4(a). The fracture energy is calculated as the products of external forces times the corresponding displacements. For specimen movement from position A to B, the fracture energy per unit crack area can be calculated as per Eq. (7) after [18-20]:

$$G_F = \frac{1}{ht}\left(2\int_{UA}^{UB} F_H(u)du + 2\int_{VA}^{VB} \frac{F_V(v)}{2} dv + mge\tan(\varphi^{AB}) \right) \tag{7}$$

where,

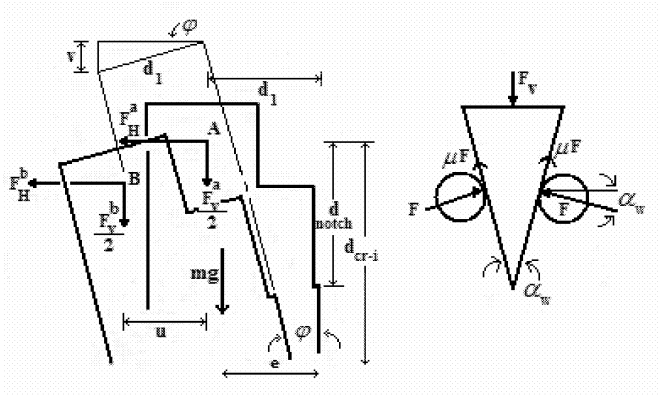

(a)

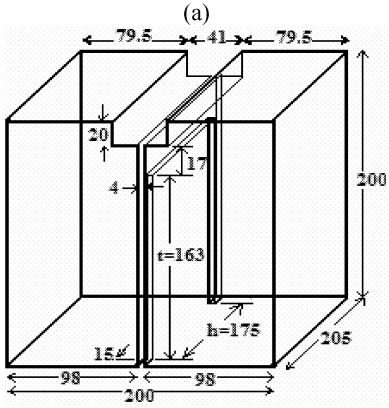

(b)

Fig. 4. (a) Force Components Applied to WST Sample (Left) and Steel Wedge (Right); (b) Dimensions of the Wedge-split Test Specimen (mm).

Table 1. Concrete Mix Proportions by Weight of the Six Specimens.

Material	Weight (kg/m^3)
Coarse Aggregate	1128.8
Sand	698.4
Cement (Type I)	316.0
Water	158.0

u is the displacement in the horizontal direction;
v is the displacement in the vertical direction;
e is the distance from the crack to the centroid of the half sample;
m is mass of sample, and g is the acceleration of gravity;
h is the length and t is the thickness of the fracture surface area, and ht gives the fracture surface area (magnitudes of h and t are given in Fig. 4(b)); and
φ^{AB} is the sample rotation from position A to B about the crack tip (see Fig. 4(a)).

Eq. (8) can be obtained from the free body diagrams of the wedge and half sample in Fig. 4(a):

$$\begin{aligned} F_V &= 2\tan\alpha_W F_H \\ dv &= d_1 d\varphi \\ \tan\varphi &= \varphi \end{aligned} \tag{8}$$

Combining Eqs. (7) and (8), the fracture energy per unit crack area can be calculated as Eq. (9), or Eq. (10) in a integrated form, assuming that A is the position at $u = 0$, $v = 0$, $\varphi = 0$ and B is the position at $u = u_{\max}$, $v = v_{\max}$ and $\varphi = \varphi_{\max}$. α_W is the wedge angle in Eq. (9). Eq. (10) was used in this study for calculating the fracture energy per unit crack area. The CMOD in Eq. (10) denotes crack mouth opening displacements.

$$G_F = \frac{1}{ht\tan\alpha_W}\int_0^{u_{\max}} F_V(u)du + \frac{d_1}{ht}\int_0^{\varphi_{\max}} F_V(\varphi)d\varphi + mged\varphi_{\max} \tag{9}$$

$$\begin{aligned} G_F = {} & \frac{1}{2ht\tan\alpha_W}[Area\ under\ F_v - CMOD] \\ & + \frac{d_1}{ht}[Area\ under\ F_v - \varphi] + \frac{mge}{ht}\varphi_{\max} \end{aligned} \tag{10}$$

Test Plan and Results

In the laboratory work of this study, six concrete specimens were fabricated using Type I cement and three types of aggregate at a w/c ratio at 0.5 as seen in the mixture proportions given in Table 1. The aggregate blends of the six concrete mixes consisted of two types of gradation, i.e., gap gradation and the dense gradation; and two maximum aggregate sizes, 38.0 mm and 25.0 mm. The aggregate types and gradation of the six mixes are given in Table 2. The *AI* and *ST* indices as well as the surface area of the aggregate particles included in each specimen were determined using image analysis in UIAIA. The *AI* and *ST* indices and surface area of the aggregate particles for the six concrete mixes can be found in Table 3. The *AI* and *ST* indices in Table 3 are the average *AI* and *ST* indices of the individual aggregate particles in each concrete specimen. It should also be noted that the surface area of the six specimens are given in terms of the surface area density that is defined as the total surface area of aggregate particles within a unit volume of concrete (m^2/m^3).

The fracture energy of six concrete mixes was determined by the wedge splitting test (WST) method [21] and presented in Table 3 also. The WST specimens were 200 mm tall and wide by 205 mm deep as shown in Fig. 4(b). The WST specimens had a 37 mm deep top notch and 15 mm deep side notches. The WST test configuration, shown in Fig. 5(a), involved loading the specimen at a constant displacement rate of 0.5 mm per minute to ensure stable crack propagation after the peak load. The configuration of the WST was developed at the University of Illinois [19, 20]. The crack mouth opening displacements (CMOD) on opposite sides of the crack and the vertical displacement of the wedge were measured using LVDTs. The load, the vertical movement of the wedge, and the CMODs were recorded every 500 milliseconds. From the measured vertical load and average CMOD, the fracture energy was calculated as per Eq. (10). Two WST samples were prepared and tested for each concrete mix after 12-hour of moisture curing. Fig. 5(b) shows the fracture surfaces of six tested specimens [19, 20].

Data Analysis

To investigate possible aggregate shape properties that might affect the early age cracking behavior of cement concrete, the angularity

Table 2. Aggregate Type and Combined Gradation (Retained on by Weight) of Six Concrete Specimens.

Sieve Size (mm)	38GTR (%)	38GRG (%)	25DTR (%)	25GRG (%)	25DRG (%)	25DLS(%)
38.1	-	-	-	-	-	-
25.4	29.3	25.7	-	-	-	-
19	9.5	26.3	13.5	6.8	13.5	13.5
12.7	11.2	5.9	17	33.9	17	17
9.5	10	0.9	10.5	14.7	10.5	10.5
4.76	-	1.2	19	4.6	19	19
Fine/Sand	40	40	40	40	40	40

38GTR = Trap rock (Basalt) of gap gradation with maximum size aggregate of 38 mm;
38GRG = River gravel of gap gradation with maximum size aggregate of 38 mm;
25DTR = Trap rock (Basalt) of Fuller gradation with maximum size aggregate of 25 mm;
25GRG = River gravel of gap gradation with maximum size aggregate of 25 mm;
25DRG = River gravel of Fuller gradation with maximum size aggregate of 25 mm;
25DLS = Dolomite of Fuller gradation with maximum size aggregate of 25 mm.

Table 3. G_F and Surface Area Density of Aggregate in the Six Concrete Specimens.

Mix ID	12-hour G_F(N/m)	Surface Area Density (m^2/m^3)	*AI* Index	*ST* Index
38GTR	194.5	1287	483	1.90
38GRG	145.8	1262	328	0.99
25DTR	114.4	2127	492	2.21
25GRG	89.1	1910	327	0.95
25DRG	87.8	2323	343	0.96
25DLS	52.7	2385	451	1.52

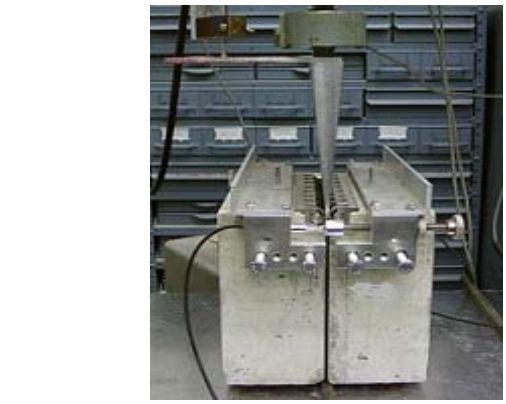

(a)

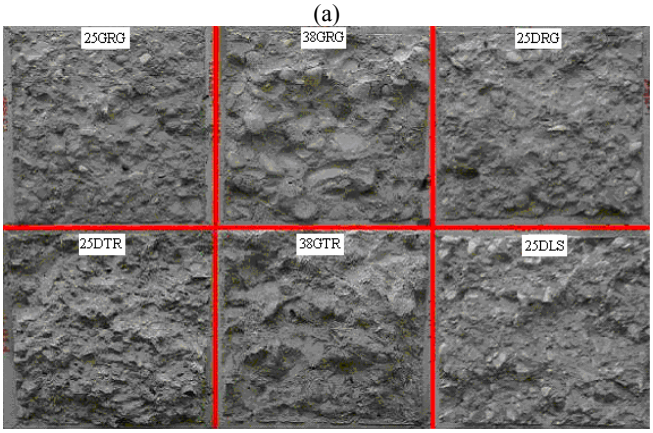

(b)

Fig. 5. (a) Wedge Split Test Specimen Setup; (b) Cracked Surfaces of the Tested Specimens.

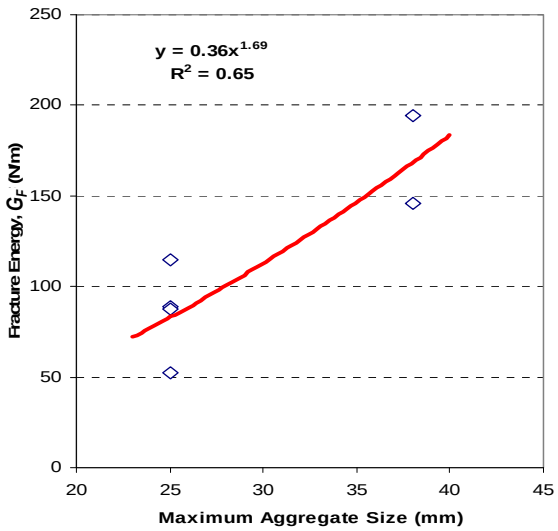

Fig. 6. Best-Fit Regression between the Fracture Energy and the Maximum Aggregate Size.

index (*AI*) and surface texture index (*ST*) of the six concrete mixes are linked to the fracture energy. Best-fit power regressions performed between the fracture energy and the indices *AI* and *ST* of aggregate for the concrete mixes generate poor coefficients of determination (R^2 = 0.01 for *AI* and R^2 = 0.05 for *ST*), which basically indicates that important aggregate shape properties, i.e., the angularity and the surface texture properties are not among the top factors that significantly affect early-age fracture behavior of concrete. Nevertheless, this conclusion needs further verification considering that only six mixes were tested in this study. Other factors such as the design of experiments with limited mixes might also contribute to this conclusion. To examine the effect of the maximum size of aggregate materials on the early-age fracture behavior of concrete, the maximum size of the six specimens are linked to the fracture energy values as show in Fig. 6. An obvious trend can be found that specimens including bigger particles possess higher fracture energy. Since there was no sign of aggregate breaking observed in the wedge split test, higher fracture energy can not be attributed to the higher resistance against tensile stress of the particles per se owing to their bigger sizes.

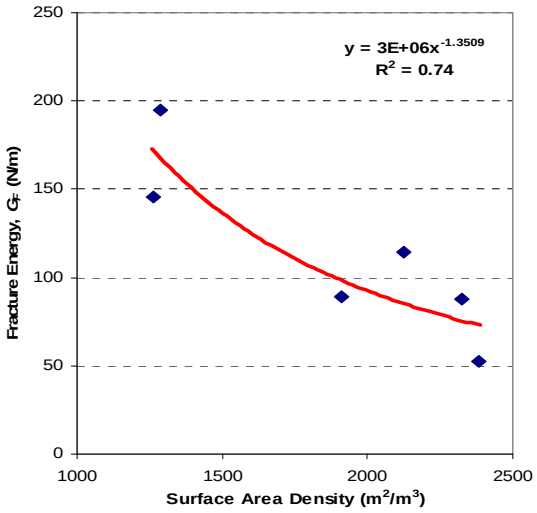

Fig. 7. Best-Fit Regression between the Fracture Energy and the Surface Area of Aggregate.

The obtruding particles and the dents left by extracted particles on the fracture surface of the concrete specimens in Fig. 5(b) show signs that fracture mainly developed in the vicinity of the particle surfaces in the concrete. Moreover, considering that the same amount of aggregate materials by weight were used in the six specimens, the specimens including aggregate materials of higher maximum size actually have low surface area density as defined in a previous part of this paper. To further verify such an observation, a best-fit regression analysis performed between the surface area density and the fracture energy values is given in Fig. 7. The coefficient of determination, 0.74, shows obviously improvement than that between the fracture energy and maximum aggregate size as shown in Fig. 6. Such a definite relationship between the surface area density and the fracture energy basically indicates that the resistance of concrete against tensile stress decreases as the surface area of the aggregate used increases. The relationship further shows that the particle surface is the weak location against tensile stress from early-age deformation of concrete structures.

Mechanism of this observation can be ascribed to the weak link between the aggregate and the paste phases, i.e., the interfacial transition zone (ITZ) that exists between the paste and aggregate phases in concrete. The ITZ has a looser microstructure compared to that of the paste and aggregate phases due to the special arrangement of cement grains in the vicinity of aggregate particle. The formation of the ITZ in young concrete has been extensively studied and the general knowledge can be used to explain the observations made in this study: the formation of the ITZ surrounding aggregate particles is initiated by the non-uniform distribution of water in the vicinity of the particles. This type of non-uniformly distributed water is caused by bleeding and/or "wall effect" that prevents effective filling of the space around aggregate particles with cement grains [22-24]. The especially loose arrangement of cement grains close to the aggregate particle surface further results in a lower level of cement hydration as compared to that happens in the paste. As a consequence, the ITZ around the aggregate particles is less effectively filled by the hydration products.

The ITZ can be further divided into two main sub-domains that have different microstructures due to different types of chemical reactions and physical changes. The inner layer of the ITZ is very thin (about 1 μm) and referred to as the "duplex" film that has calcium hydroxide ($Ca(OH)_2$) on the aggregate side and calcium silicate hydrate (C-S-H) on the cement paste side [6, 25]. The outer layer of the ITZ is about 50 ~ 100 μm thick which has a less dense structure than the bulk paste outside of the ITZ. Research studies have shown that from the aggregate-paste interface, there exists a microstructural gradient extending some 50 μm into the cement paste, the amount of anhydrous cement, $Ca(OH)_2$, C-S-H as well as density all decrease [23]. It is the loose packing of cement grains and the comparatively low cement hydration in the ITZ that mainly determines the early-age cracking behavior of Portland cement concrete as observed in this study.

It is noteworthy that the aggregate chemical composition might also affect early-age cracking behavior of concrete in this study. Compared to the significant role the aggregate surface plays in the fracture behavior of young concrete, the effects of the chemical compositions of aggregate materials on the mechanical properties of the ITZ are somewhat controversial. Research studies have reported that aggregate-cement bond was proportional to the silica content of aggregate [6]. Other studies however found that the aggregate chemical composition has little effect on the microstructure gradients and the mechanical properties of the ITZ [24]. A general recognition has been that the aggregate chemical composition is secondary to the aggregate shape and surface area in affecting the early-age cracking behavior of concrete [26, 27]. The deviation of the data points from the best fit regression curve in Fig. 7 may be explained by the effect of the aggregate chemical composition and potentially other random errors as well considering that the six specimens were subjected to many influential factors. A better correlation can be expected to achieve when more data are obtained, which is beyond the scope of this study and is not further discussed in this paper.

Conclusions

This paper presents findings of a study on the early-age fracture toughness of concrete using the fracture energy (G_F) approach, with emphasis on investigating the effects of aggregate size and shape properties on the response of interfacial transition zone (ITZ) to tensile stress. Six concrete specimens were fabricated using a Type I cement and five different types of aggregate at the w/c ratio of 0.5. G_F of the six specimens were obtained from the wedge-split tests after 12-hour of moist curing.

The angularity and surface texture properties as quantified respectively by the imaging-based *AI* and *ST* indices showed no measurable effects on the fracture energy; however, the interfacial transition zone (ITZ) was determined to be the weak places in young concrete through which early age cracking could develop, as indicated by the decent correlations of the fracture energy to both maximum aggregate size and surface area of aggregate. With the increase of aggregate surface area in concrete, the resistance of concrete specimens against tensile stress tended to decrease due to the low aggregate-paste bond strength and toughness in the ITZ compared to those of aggregate and paste. A possible mechanism

was finally proposed based on the previous research findings to explain the observations from this study. The authors believe that the mechanical properties of ITZ is significantly responsible for the response of concrete structures to tensile stress in early ages, which could be caused by the loose packing of cement grains in the vicinity of aggregate particles and the lower level of cement hydration compared to that in normal cement paste.

References

1. Schoppel, K. and Springenschmid, R., (1995). The Effect of Thermal Deformation, Chemical Shrinkage and Swelling on Restraint Stresses in Concrete at Early Ages, *Proceedings of the International RILEM Symposium: Thermal Cracking in Concrete at Early Ages*, London, UK, pp. 213-228.
2. Hillerborg, A., (1985). The Theoretical Basis of a Method to Determine the Fracture Energy G_F of Concrete, *Fatigue & Fracture of Engineering Materials and Structures*, Oxford, UK. 18(106), pp. 291-296.
3. Choubane, B., Wu, C.L. and Tia, M., (1996). Coarse Aggregate Effects on Elastic Moduli of Concrete, *Transportation Research Record*, No. 1547, pp. 29-34.
4. Mindess, S. and Young, F., (1981). *Concrete*, Prentice Hall, Englewood Cliffs, NJ.
5. Alexander, K.M. and Taplin, J.H., (1962). Concrete Strength, Bond Strength, Cement Hydration and Mature Rules, *Australia Journal of Applied Science*, 13(4), pp. 277-284.
6. Alexander, K.M., Wardlaw, J., and Gilbert, D.J., (1965). Aggregate-Cement Bond, Cement Paste Strength and the Strength of Concrete, *London Cement and Concrete Association, Proceedings of International Conference on the Structure of Concrete*, pp. 59-81, London, UK.
7. Davey, N., (1954). Concrete Mixes for various Building Purposes. *Proceedings of a Symposium on Mixes Design and Quality Control of Concrete*, London, UK, Cement and Concrete Association, pp. 28-41.
8. Hsu, T.T.C. and Slate, F.O., (1963). Tensile Bond Strength between Aggregate and Cement Paste of Mortar, *Journal of American concrete Institute*, 60(4), pp. 465-486.
9. Scrivener, K.L. and Pratt, P.L., (1996). Characterization of Interfacial Microstructure. *Interfacial Transition Zone in Concrete*, *State-of-Art Report by RILEM*, pp. 1-16.
10. Tschegg, E.K., Rotter, H.M., Roelfstra, P.E., Bourgund, U. and Jussel, P., (1994). Fracture Mechanical Behavior of Aggregate-Cement Matrix Interfaces, *Journal of Materials in Civil Engineering*, 7(4), pp. 199-203.
11. Tutumluer, E., Rao, C., and Stefanski, J.A., (2000). Video Image Analysis of Aggregates, Final Project Report, FHWA-IL-UI-278, *Civil Engineering Studies UILU-ENG-2000-2015*, University of Illinois Urbana-Champaign, Urbana, IL.
12. Pan, T. and Tutumluer, E., (2007). Imaging-based Quantification of Coarse Aggregate Surface Texture, *ASTM Journal of Testing and Evaluation*, 35(2), pp. 1-10.
13. Tutumluer, E. and Pan, T., (2008). Aggregate Morphology Affecting Strength and Permanent Deformation Behavior of Unbound Granular Materials, *ASCE Journal of Materials in Civil Engineering*, 20(9), pp. 617-627.
14. Pan, T., Tutumluer, E., and Anochie, B.J., (2006). Aggregate Morphology Affecting Resilient Behavior of Unbound Granular Materials, *Transportation Research Record*, No. 1952, pp. 12-20.
15. Pan, T., Tutumluer, E., and Carpenter, S.H., (2006). Effect of Coarse Aggregate Morphology on Permanent Deformation Behavior of Hot Mix Asphalt, *ASCE Journal of Transportation Engineering*, 132(7), pp. 580-589.
16. Pan, T., Tutumluer, E., and Carpenter, S.H., (2005). Effect of Coarse Aggregate Morphology on Resilient Modulus of Hot Mix Asphalt, *Transportation Research Record*, No. 1929, pp. 1-9.
17. Pan, T. and Tutumluer, E., (2010). Imaging-Based Direct Measurement of Aggregate Surface Area and Its Application in Asphalt Mixture Design, *International Journal of Pavement Engineering*, 11(5), pp. 415-428.
18. Østergaard, L., (2003). *Early-Age Fracture Mechanics and Cracking of Concrete - Experiments and Modeling*, Ph.D. thesis, Department of Civil Engineering, Technical University of Denmark.
19. Chupanit, P., (2005). *Characterization of Concrete Pavement Joint Surfaces*, Ph.D. Dissertation, University of Illinois, Urbana-Champaign.
20. Chupanit, P. and Roesler, J.R. (2008). Fracture Energy Approach to Characterize Concrete Crack Surface Roughness and Shear Stiffness, *Journal of Materials in Civil Engineering*, 20(4), pp. 275-282.
21. Tschegg, E.K., (1991). New Equipment for Fracture Tests on Concrete, *Material Testing*, Vol. 33, pp. 338-342.
22. Diamond, S., (1986). The Microstructure of Cement Paste in Concrete, *Proceedings of the 8th International Congress on the Chemistry of Cement*, Rio de Janeiro, Vol. I, pp. 122-147.
23. Scrivener, K.L., Bentur, A. and Pratt, P. L., (1988). Quantitative Characterization of the Transition Zone in High Strength Concretes, *Advances in Cement Research*, 1(4), pp. 230-237.
24. Hoshino, M., (1989). Relation between Bleeding, Coarse aggregate and Specimen Height of Concrete, *Journal of American Concrete Institute*, Vol. 86, pp. 185-190.
25. Barnes, B.D., Diamond, S. and Dolch, W.L., (1979). Micromorphology of the Interfacial Zone around Aggregates in Portland Cement Mortar, *Journal of the American Ceramic Society*, Vol. 62, pp. 21-24.
26. Odler, I. and Zurz, A., (1988). Structure and Bond Strength of Cement-Aggregate Interface, *Bonding in Cementitious Composites*. Materials Research Society, Vol. 114, pp. 21-27.
27. Bentur, A. and Odler, I., (1996). Development and Nature of Interfacial Microstructure, *Interfacial Transition Zone in Concrete. State-of-Art Report by RILEM*, pp. 19-44.